

SPATIO-TEMPORAL CHARACTERISTICS OF TURBULENT FLOW SEPARATIONS AROUND RECTANGULAR AND TRAPEZOIDAL PRISMS IN UNIFORM FLOW

Sedem Kumahor

Department of Mechanical Engineering
University of Manitoba
Winnipeg, Manitoba, R3T 5V6, Canada
kumahors@myumanitoba.ca

Xingjun Fang

Department of Mechanical Engineering
University of Manitoba
Winnipeg, Manitoba, R3T 5V6, Canada
fangx@myumanitoba.ca

Mark F. Tachie

Department of Mechanical Engineering
University of Manitoba
Winnipeg, Manitoba, R3T 5V6, Canada
mark.tachie@umanitoba.ca

ABSTRACT

Turbulent flow separations over rectangular prisms of streamwise aspect ratios of 1 (AR1) and 2 (AR2), and a trapezoidal prism were experimentally studied using time-resolved particle image velocimetry at a Reynolds number (based on free-stream velocity and prism height) of 16200. The trapezoidal prism has a 45° inclined trailing face and its upper and lower streamwise lengths are, respectively, identical to those of the AR1 and AR2 prisms. The mean flow, vortex shedding motions and spatial characteristics of the symmetric and asymmetric wakes produced by the rectangular and trapezoidal prisms, respectively, are investigated in terms of turbulent statistics, frequency spectrum and two-point autocorrelation. The results indicate that the mean recirculation bubble and magnitudes of the Reynolds stresses in the wake region of the trapezoidal prism are in close agreement with AR2, indicating the dominance of the shear layer from the longer side of the trapezoidal prism. The fundamental shedding frequency for the trapezoidal prism and its harmonic are intermediate to those observed for the rectangular prisms. Two-point autocorrelation analyses reveal a higher structural coherency between the wake vortex and small-scale vortices formed at the leading edge of AR2 prism compared to AR1 and the trapezoidal prism. Spectral proper orthogonal decomposition analyses also reveal the coherent structures that occur at the dominant and sub-dominant shedding frequencies.

INTRODUCTION

Transport phenomena and vortex shedding motions in turbulent flows over symmetric bluff bodies such as rectangular prisms in uniform flows have been critically examined over the past decades. The turbulent statistics, drag characteristic and vortex shedding motions strongly depend on the streamwise aspect ratio ($AR = L/h$, where L and h represent the streamwise length and vertical height of the prism, respectively). The fundamental vortex shedding frequency ($St = fh/U_e$, where f is the dominant frequency and U_e is the free-stream velocity), for example, decreases from 0.13 to 0.08 as the aspect ratio increases from 1 to 2 (Okajima, 1982, Knisely, 1990; Norberg, 1993). Meanwhile, the peak Reynolds normal stresses in the near wake region of a square prism are an order of magnitude higher than the corresponding values for a rectangular prism with an aspect ratio of 2 (Nakagawa et al. 1999).

The differences in the vortex shedding dynamics and mean flow topology for AR2 compared to AR1 have been

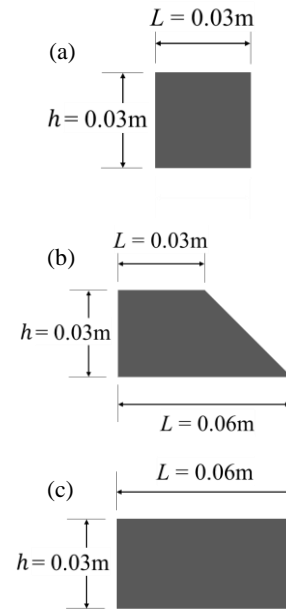


Figure 1: Cross-sectional view of the AR1 prism (a), trapezoidal prism (b) and AR2 prism.

attributed to the intermittent reattachment of the shear layer on to the body surface (Okajima, 1982; Nakagawa et al. 1999). Consequently, there is significant narrowing and widening of the wake vortices shed from the trailing edge of the AR2 prism. Recent experimental investigations by Mohebi et al. (2017) for $AR = 1.92$ also showed a significantly larger wake recirculation region compared to the square cylinder (AR1). They argued that the trailing edge flow dynamics plays an important role in the vortex formation and shedding process around rectangular prisms.

In this study, the sharp trailing edge of the AR2 prism is replaced by a 45° inclined face, creating a trapezoidal prism as shown in Figure 1(b). This modification results in a prism with upper and lower streamwise lengths corresponding to 1 and 2 times the prism heights, respectively, and an introduction of geometrically-imposed asymmetry on the flow dynamics. The objective of the present study is to investigate the spatio-temporal features of symmetric wake flows produced over rectangular prisms of aspect ratios of 1 (Figure 1(a)) and 2 (Figure 1(c)), and an asymmetric wake flow over a trapezoidal prism (Figure 1(b)) using time-resolved particle image velocimetry (TR-PIV). The results are analysed in terms of the mean velocity, Reynolds stresses, frequency

spectra and two-point correlation. The large-scale coherent flow structures are also extracted and analysed using spectral proper orthogonal decomposition (SPOD)

EXPERIMENTAL SET-UP

The experiments were performed in an open recirculating water channel at the University of Manitoba. The streamwise length, spanwise width and vertical height of the test section are 6.0 m, 0.6 m and 0.45 m, respectively. Two rectangular prisms and a trapezoidal prism with vertical height, $h = 0.03$ m and spanwise width, $B = 0.58$ m were investigated. As shown in Figure 1, the streamwise lengths of the rectangular prisms are 0.03 m (AR1) and 0.06 m (AR2) while the streamwise lengths of the upper and lower sides of the trapezoidal prism are 0.03 and 0.06 m, respectively. The water depth was kept constant at 0.43 m and the prisms were positioned such that the prism mid-height was 0.215 m above the bottom wall. The measured boundary layer thickness was 0.065 m and hence the prism was exposed to uniform oncoming flow. The free-stream velocity was set to $U_e = 0.540$ m/s and the Reynolds number was 16200.

Time-resolved particle image velocimetry (TR-PIV) was used to perform velocity measurements at the mid-span of the channel. The water was seeded with 10 μ m silver coated hollow glass spheres of specific gravity, 1.4. A diode pumped dual-cavity high-speed Neodymium-doped yttrium lithium fluoride (Nd:YLF) laser with maximum pulse energy of 30 mJ/pulse for each cavity was used to illuminate the seeding particles. Two high speed 12-bit complementary metal oxide semiconductor cameras of resolution, 2560 pixel \times 1600 pixel positioned side-by-side were used to image the flow in two fields of view (FOV) simultaneously. The dimensions of the FOVs over the rectangular prisms and wake region were, respectively, $3.3h \times 2.1h$ and $4.6h \times 2.9h$, resulting in digital image resolutions of 25.0 pixel/mm and 18.4 pixel/mm, respectively. For the trapezoidal prism, the FOVs over the prism and in the wake region were, respectively, $2.7h \times 1.7h$ and $7.3h \times 4.6h$, resulting in digital image resolutions of 31.8 pixel/mm and 11.7 pixel/mm, respectively. These spatial resolutions were chosen such that the flow interactions between the leading and trailing edges are resolved in the first FOV and the large wake recirculation region are resolved in the second FOV.

The sampling frequency was set to 800 Hz and 96000 images were captured for each test case. Data acquisition and image post-processing were performed using commercial software (DaVis version 10.0.5) supplied by LaVision Inc. Velocity vectors were calculated using a GPU-accelerated multi-pass cross-correlation algorithm with a single initial pass of 128 pixel \times 128 pixel interrogation area (IA) with 50% overlap followed by four final passes of 24 pixel \times 24 pixel IA with 75% overlap.

RESULTS AND DISCUSSION

Contour plots of the streamwise mean velocity superimposed with the mean streamlines are shown in Figure 2 to visualize the mean flow over the prisms. The approach flow accelerates past the prisms with local maximum velocity at a location approximately above the highest point of the mean separating streamline. The value of maximum velocity over the trapezoidal prism is lower compared to the rectangular prisms due to the topological differences in the mean flow over the prisms. Specifically, the mean streamlines

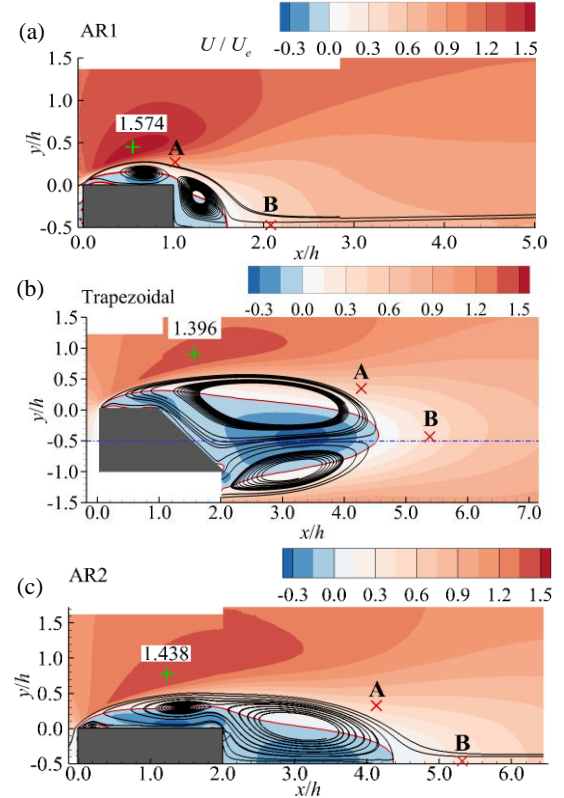


Figure 2: Streamwise mean velocity (U) superimposed with representative mean streamlines and the isopleth of $U = 0$. Symbol + marks the peak with the value written above. Locations A and B marked using \times represent the locations of peak $\overline{u'u'}$ and $\overline{v'v'}$, respectively.

reveal distinct mean recirculation bubbles over the rectangular prisms, but not over the trapezoidal prism. The streamwise extent of mean flow reversal within the wake region (L_R), as indicated by the isopleth of $U = 0$, is significantly shorter in the AR1 case ($L_R/h = 1.6$) compared to AR2 and trapezoidal prisms ($L_R/h \sim 4.2$). The value of $L_R/h = 1.6$ for AR1 is in good agreement with that reported by Trias et al. (2015). Near the upper trailing edges, the maximum magnitudes of the mean backflow were $U/U_e = 0.08$, 0.29 and 0.25 for the AR1, AR2 and trapezoidal prisms, respectively. This backflow toward the leading edge of the prisms creates an adverse pressure gradient leading to the formation of a small secondary recirculation bubble near the leading edge of the prisms (Trias et al., 2015; Kumahor and Tachie, 2022). The well-resolved secondary recirculation bubbles close to the leading edge of the prisms are indicative of the fine spatial resolution adopted in this study.

The contours of the Reynolds shear stress ($\overline{u'v'}$) around the prisms are compared in Figures 3. A distinct region of positively valued $\overline{u'v'}$ is evident close to the leading edge ($x/h < 0.5$), regardless of prism geometry. This is induced by misalignment of the Cartesian coordinate with local mean streamlines (Fang and Tachie, 2019). There exist dual local peaks of $\overline{u'v'}$ within the wake region. It is noted that the magnitudes of peak Reynolds shear stress and Reynolds normal stresses (not shown) in the AR1 case are consistently larger than the other two prisms. The stronger Reynolds stresses in the AR1 case promote entrainment of free-stream flow into the wake flows and thus reduce the size of the mean recirculation bubble as shown in Figure 2(a). Figures 2 and 3 clearly show that the mean flow topology including the recirculation length as well as the magnitude of Reynolds

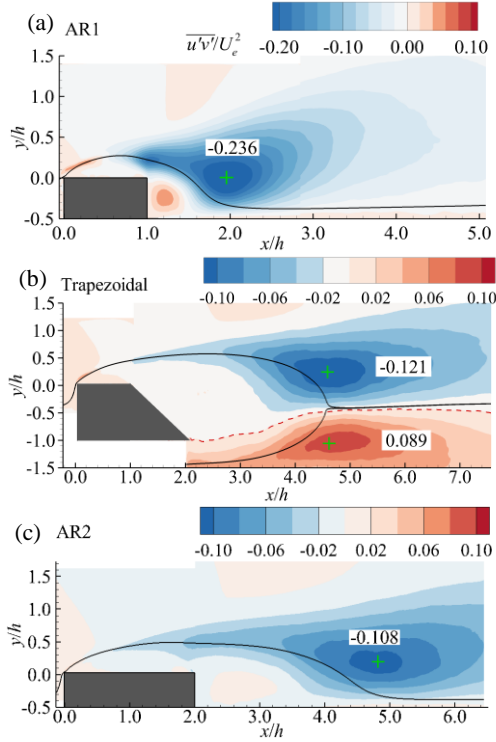


Figure 3: Reynolds shear stress ($\overline{u'v'}$) superimposed with the mean separating streamline. Symbol + marks the peak with the value written beside it.

stresses and their streamwise locations for the trapezoidal prism are in closer agreement with AR2 than the AR1 prism. These similarities between the trapezoidal and AR2 prisms suggest the dominance of the shear layer from the longer side of the trapezoidal prism on the mean flow and turbulent statistics in the near wake region.

Figure 4 presents the frequency spectra of the streamwise and vertical fluctuating velocities at the peak locations of $\overline{u'u'}$ (point A) and $\overline{v'v'}$ (point B). All spectra exhibit the $-5/3$ slope over a wide range of frequencies, reflecting a well-resolved inertial subrange at high Reynolds numbers. At the peak location of $\overline{u'u'}$, the fundamental von-Kármán (VK) vortex shedding frequencies for the AR1, AR2 and trapezoidal prisms are $St_{VK} = 0.138$, 0.084 and 0.104 , respectively. The dominance of these frequencies is also evident in ϕ_{vv} at the peak location of $\overline{v'v'}$. The dominant frequencies for the rectangular prisms agree well with fundamental shedding frequencies reported for AR1 and AR2 in previous investigations (Okajima, 1982; Knisely, 1990; Norberg, 1993). Meanwhile, the $St_{VK} = 0.104$ for the trapezoidal prism is midway between the corresponding values for the two rectangular prisms. The spectra also revealed peaks at the 2nd and 3rd harmonics, although the peaks at the harmonics are more prominent for AR1 compared to the other prisms. For the AR2 case, a peak value at $St = 0.142$ (which is lower than the 2nd harmonic) is also observed which is consistent with the findings by Knisely (1990) and Norberg (1993). The existence of these two frequencies for the AR2 case have been previously attributed to the intermittent reattachment of the separated shear layer onto the prism surface. Consequently, there is a dual vortex shedding process evidenced in the significantly larger wake recirculation region observed in Figure 2.

Figure 5 examines the spatial structures using two-point autocorrelations of the streamwise fluctuating velocity. Here,

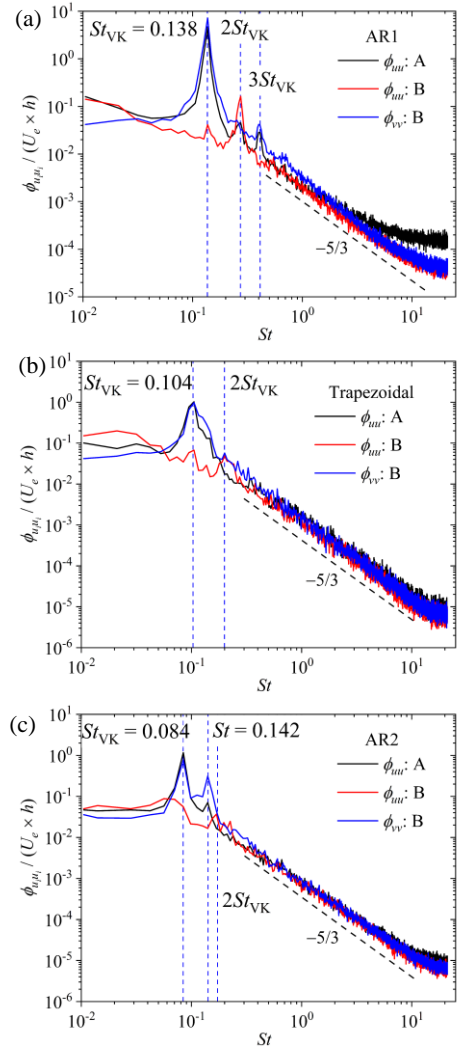


Figure 4: Frequency spectra of the streamwise fluctuating velocity (ϕ_{uu}) and vertical fluctuating velocity (ϕ_{vv}) at the locations of peak $\overline{u'u'}$ (A) and peak $\overline{v'v'}$ (B) as marked in Figure 2 for the AR1 (a), trapezoidal (b) and AR2 (c) prisms.

the reference point is chosen to be $0.1h$ above the trailing edge and the mean separating streamline are superimposed to examine the feedback influence of the large-scale wake vortex on the small-scale vortices formed near the leading edge of the prisms. Downstream of the reference point, the isopleths of correlation coefficient (R_{uu}) extend towards the symmetry plane but decorrelate more rapidly in the wake of AR2 prism. This suggests that the vortices passing the reference point tends to maintain their structural integrity so as to interlink the dynamics of unsteadiness near the separating point and wake region in the AR1 and trapezoidal cases. In the AR2 case, on the other hand, the flow structure experiences a longer developing distance over the bluff body and thus dominates over the influence of the structure in the wake region. Upstream of the reference point, the correlation coefficient decays more slowly over the AR2 prism compared to AR1 and trapezoidal prisms. Additionally, the levels of correlations near the separating streamline over the AR1 and AR2 prisms are significantly higher compared to the trapezoidal prism. In the case of the trapezoidal prism, for instance, the decorrelation point along the mean separating streamline (which is defined as the intersection of the mean streamline and the isopleth of $R_{uu} = 0$) is only $0.5h$ (i.e., $x/h = 0.5$) from

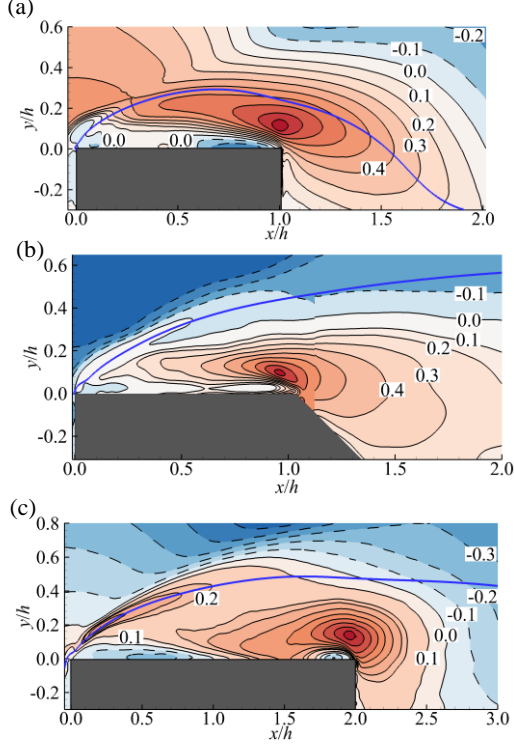


Figure 5: Two-point autocorrelation of the streamwise fluctuating velocity (R_{uu}) for the AR1 (a), trapezoidal (b) and AR2 (c) prisms. with the reference points $0.1h$ above the trailing edge. Blue continuous line represents the mean separating streamline and the contours levels shown are in 0.1 increments.

the self-correlation point compared to $0.95h$ (i.e., $x/h = 0.05$) for the AR1. For the AR2 prism, correlation coefficient as high as $R_{uu} = 0.4$ are evident in the vicinity of the leading edge. These observations suggest that the interaction between wake vortex and vortices near the separating point is the weakest in the trapezoidal case. In fact, the correlations in both AR1 and AR2 cases are still significant upstream of the separating point, especially for the former one.

Spectral proper orthogonal decomposition (SPOD), proposed by Sieber et al. (2016) was performed for the flow around the tested prisms. This method, which is an extension of the snapshot POD method (Sirovich, 1987) decomposes the phenomena occurring at multiple frequencies and energies using a spectral filter. This enables a clear separation of spatially and temporally coherent structures into a series of spectral modes that represent the flow physics. Detailed formulation and application of the technique to various TR-PIV datasets are presented in Sieber et al. (2016).

The premultiplied frequency spectra of the first two spatial mode coefficients are presented in Figure 6. Consistent with the findings by Sieber et al. (2016) for periodic vortex shedding motions, the dominant frequencies in the spectra of the first SPOD mode correspond to the fundamental von-Kármán (VK) vortex shedding frequencies presented in Figure 4 for the rectangular prisms. Comparing the spectral energy content for the first and second modes, all the spectral peaks for the first mode are more than tenfold of the second mode. This suggests that the major flow coherency is presented in the first mode and hence attention is focused solely on the first mode hereinafter. For AR1, the second and third harmonic frequencies of the fundamental vortex shedding frequency ($St_{VK} = 0.138$) are evident as sub-dominant peaks in the

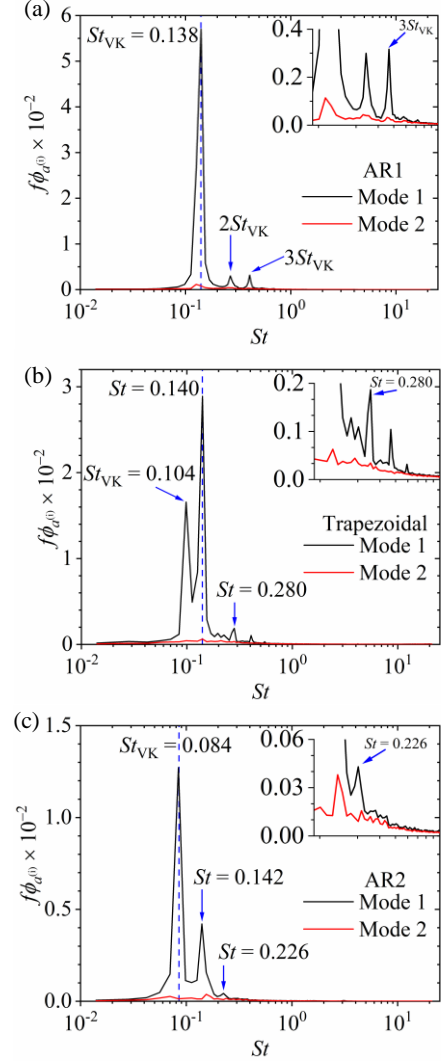


Figure 6: Premultiplied frequency spectra of the first two spatial POD mode coefficients ($\phi_{\alpha(i)}$) for the AR1 (a), trapezoidal (b) and AR2 (c) prisms. The high frequency variations are shown clearly using figure inserts at the top right corner.

spectra (see Figure 6(a)). For AR2, two distinct shedding frequencies are observed, with dominance at $St_{VK} = 0.084$ and sub-dominance at $St = 0.142$. The existence of the dual vortex shedding frequencies corroborates the findings by previous investigations (Okajima, 1982; Knisely, 1990; Norberg, 1993). For the trapezoidal prism, the dominant frequency ($St = 0.140$) is weakly observed in Figure 4(b), meanwhile, the fundamental shedding frequency ($St_{VK} = 0.084$) is the sub-dominant peak in the spectra presented in Figure 6(b). This observation suggests that the trapezoidal prism also undergoes a dual vortex shedding process, similar to the AR2 prism. It is interesting to note that the dominant peak ($St = 0.140$) is similar to fundamental shedding frequency for AR1 ($St_{VK} = 0.138$) and the sub-dominant peak for AR2 ($St = 0.142$).

The SPOD modes at selected phases at the dominant and sub-dominant frequencies are presented in Figure 7. For AR1, the coherent structure at $St_{VK} = 0.138$ represents the alternate vortex shedding process which is symmetric about the prism centerline (Figure 7(a)). At $2St_{VK}$, the structures resulting from vortex break up and an alteration of the vortex shedding process are observed in Figure 7(b). In this case, the vortex

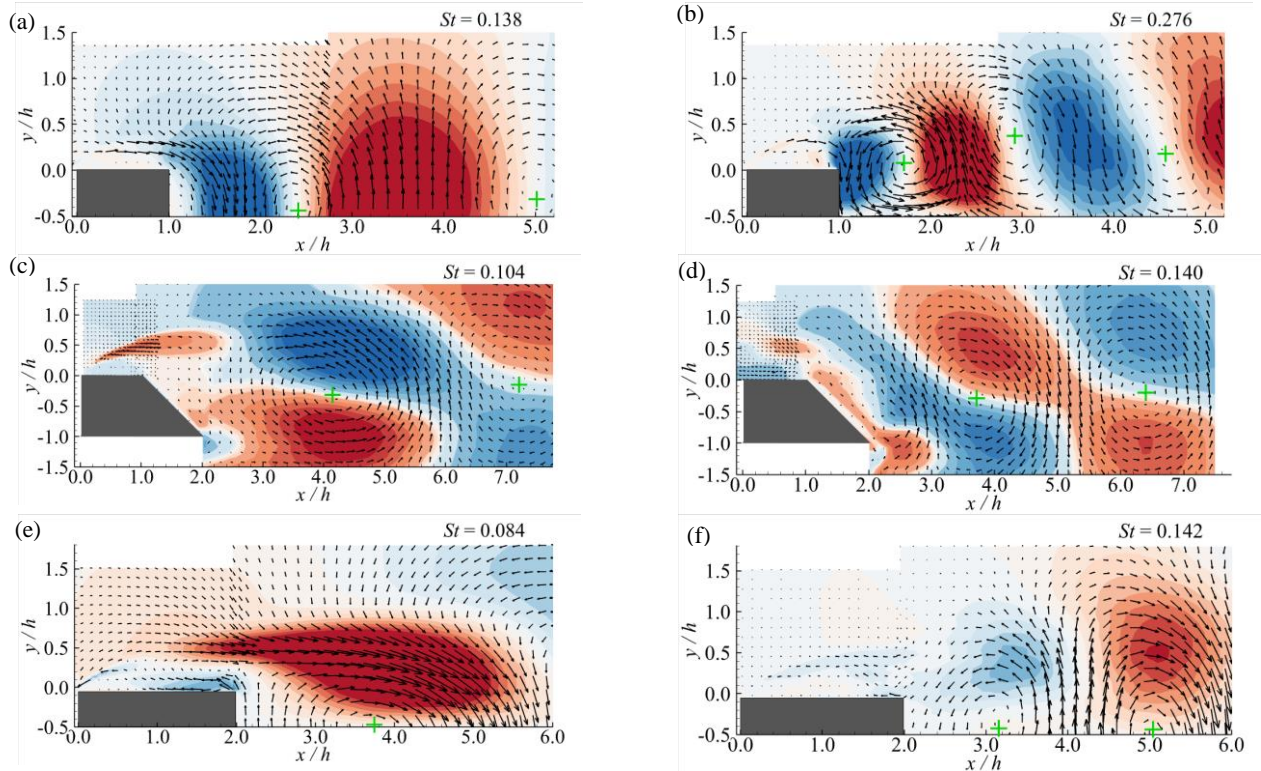


Figure 7: Contours of the first two dominant SPOD modes using the streamwise velocity fluctuations (u') for AR1 (a,b), trapezoidal (c,d) and AR2 (e,f) prisms. The symbol (+) represents the vortex centers.

cores are off-centered and the wavelength (defined as the streamwise distance between the vortex cores) is approximately half that at St_{VK} . For AR2, a large coherent structure emanating from the leading edge is convected into the wake region at $St_{VK} = 0.084$ (Figure 7(e)). Near the trailing edge, the flow is observed to bump upward and flow upstream, indicating that the separated shear layer is not reattached. Thus, the flow structure occurring at $St_{VK} = 0.084$ is shown to correspond to the instance when the wake width is wide, and the separated shear layer is not reattached. At $St = 0.142$, the spatial modes emanate from the trailing edge and are concentrated within the wake region, suggesting that the vortex shedding is occurring from the trailing edge and the separated shear layer is reattached onto the surface of the prism. The evidently higher spectral energy content of $St_{VK} = 0.084$ (Figure 6(c)) and the significantly larger wavelength is responsible for the large recirculation region around the AR2 prism. It is important to note that, the vortex cores for both frequencies are located along the prism centerline, indicating the symmetric nature of the dual vortex shedding process for AR2. For the trapezoidal prism, the dominant peak ($St = 0.140$) reveals coherent structures that are aligned at an angle of 45° , corresponding to the angle of inclination of the trailing face. At $St = 0.104$, the coherent structures emanate from the leading edge and the vortex cores are apparently aligned at approximately the prism mid-height. Furthermore, the wavelengths in both Figures 7(c,d) are identical.

CONCLUSION

A time-resolved particle image velocimetry technique was used to investigate the turbulent flow characteristics over rectangular prisms of streamwise aspect ratios of 1 (AR1) and

2 (AR2), and a trapezoidal prism in uniform flow. The trapezoidal prism had a 45° inclined trailing face that resulted in its upper and lower streamwise lengths corresponding to those of the AR1 and AR2 prisms, respectively. The Reynolds number based on the free-stream velocity and prism height was 16200.

Contours of the streamwise mean velocity show mean flow separation at the sharp leading edge for all tested prisms, meanwhile, the value of maximum velocity over the trapezoidal prism is lower compared to the rectangular prisms. The mean streamlines also showed that the mean recirculation bubble over the trapezoidal prism is suppressed due to the modified trailing edge. Two-point correlation analyses show that the interaction between wake vortex and vortices near the leading edge is weakest over the trapezoidal prism. The stronger magnitude of Reynolds stresses in the AR1 case promotes entrainment of free-stream flow into the wake flows and hence reduces the size of the mean recirculation bubble. On the other hand, the recirculation length of the mean recirculation bubble in the wake for AR2 and the trapezoidal prism are similar.

Dual vortex shedding frequencies are observed over the AR2 and trapezoidal prisms, while a single dominant shedding frequency is observed for AR1. Spectral proper orthogonal decomposition shows that the dominant and sub-dominant frequencies in AR2 correspond to a wide and narrow wake width, respectively, which are a consequence of the intermittent reattachment of the shear layer onto the prism. For the trapezoidal prism, the dominant and sub-dominant frequencies show coherent structures that are aligned at a 45° angle and in the streamwise direction, respectively. The size of the vortices formed at the dominant frequency for AR2 and the trapezoidal prism are similar, suggesting the dominance of

the shear layer from the longer (AR2) side of the trapezoidal prism on the wake flow dynamics.

ACKNOWLEDGMENT

The funding support from the Natural Sciences and Engineering Research Council of Canada (NSERC), to MFT is gratefully acknowledged. We are also grateful to Canada Foundation for Innovation for funding for the experimental facility.

REFERENCES

- Fang, X., and Tachie M. F., 2019a, "Flows over surface-mounted bluff bodies with different spanwise widths submerged in a deep turbulent boundary layer", *Journal of Fluid Mechanics*, Vol 877, pp. 717-758
- Knisely, C. W., 1990, "Strouhal numbers of rectangular cylinders at incidence: a review and new data", *Journal of Fluids and Structures*, Vol. 4, pp. 371-393.
- Kumahor, S., and Tachie M. F., 2022, "Turbulent flow around rectangular cylinders with different streamwise aspect ratios". *Journal of Fluids Engineering*, Vol. 144, pp. 051304.
- Lander, D. C., Moore, D. M., Letchford, C. W., and Amitay, M., 2018, "Scaling of square-prism shear layers", *Journal of Fluid Mechanics*, Vol. 849, pp. 1096-1119.
- Mohebi, M., Plessix, P., Martinuzzi, R. J., and Wood, D. H., 2017, "Effect of thickness-to-chord ratio on the wake of two-dimensional rectangular cylinders". *Physical Review Fluids*, Vol 2, pp. 064702.
- Nakagawa, S., Nitta, K., and Senda, M., 1999, "An experimental study on unsteady turbulent near wake of a rectangular cylinder in a channel flow", *Experiments in Fluids*, Vol. 27, pp. 284-294.
- Norberg, C., 1993, "Flow around rectangular cylinders: Pressure forces and wake frequencies", *Journal of Wind Engineering and Industrial Aerodynamics*, Vol. 49, pp. 187-196.
- Okajima, A., 1982, "Strouhal numbers of rectangular cylinders", *Journal of Fluid Mechanics*, Vol 123, pp. 379-398.
- Sieber, M., Paschereit, C. O., and Oberleithner, K., 2016, "Spectral proper orthogonal decomposition". *Journal of Fluid Mechanics*, Vol. 792, pp. 798-828.
- Sirovich, L., 1987, "Turbulence and the dynamics of coherent structures. Part I, II and III". *Quarterly of Applied Mathematics*, Vol. 45, pp. 561-571.
- Trias, F. X., Gorobets, A., and Olivia, A., 2015, "Turbulent flow around a square cylinder at Reynolds number 22,000: A DNS study", *Computers and Fluids*, Vol. 123, pp. 87-98